

# SIMULATION TECHNIQUES IN HYPERSONIC AEROTHERMODYNAMICS

**Vladimir V. Riabov**  
**Rivier College, Nashua, New Hampshire 03060, USA**

**Keywords:** *hypersonic non-equilibrium rarefied-gas flows, aero- & thermodynamic coefficients*

## Abstract

*Hypersonic viscous flows near simple-shape bodies (wedge, cone, disk, plate, sphere, and rotating cylinder) have been studied under the conditions of wind-tunnel experiments and hypersonic flights. The Direct Simulation Monte-Carlo technique has been used to study the influence of similarity parameters on aerodynamic coefficients in hypersonic streams of air, nitrogen, helium, and argon. It has been found that, for conditions approaching the hypersonic stabilization limit, the Reynolds number and temperature factor are primary similarity parameters. The influence of other parameters (specific heat ratio, Mach number, and viscosity parameter) becomes significant at low Reynolds numbers (less than 10) and small values of the hypersonic similarity parameter (less than 1). The numerical results are in a good agreement with experimental data, which were obtained in a vacuum chamber at Reynolds numbers from 0.1 to 200. The effect of nonequilibrium processes on simulation of these flows over blunt bodies has been studied by solving the full Navier-Stokes equations and the viscous-shock-layer equations. The nonequilibrium, equilibrium and "frozen" flow regimes have been examined for various physical and chemical processes in air and nitrogen, including excitation of rotational degrees of molecular freedom, chemical reactions and ionization. It has been found that the binary similitude law is satisfied for blunt bodies in the transition flow regime.*

## 1 Introduction

Planetary exploration programs [1] stimulate new studies in hypersonic high-temperature gas dynamics. Similarity principles play a fundamental role in applied aerodynamics. In a context of hypersonic viscous flow research, these principles were discussed in reviews of Cheng [2], Koppenwallner [3], Gusev [4], and Anderson [5]. Similarity criteria for hypersonic flows in the transitional rarefied gas flow regime, which lies between continuum and free molecular flow, were defined by Gusev *et al* [6]. Unfortunately, at this time, it is impossible to completely simulate high-altitude flight conditions in hypersonic wind tunnels (see notes in Ref. 4). Nevertheless, the technique of partially simulating the major criteria gives valuable information about aerothermodynamic characteristics for hypersonic vehicle designers. These studies indicate that the main criterion of similarity is the Reynolds number  $Re_0$ , in which the viscosity coefficient is calculated by means of the stagnation temperature. The influence of other similarity parameters (temperature factor  $t_w$ , specific heat ratio  $\gamma$ , viscosity parameter  $n$ , upstream Mach number  $M_\infty$ , and hypersonic parameter  $K = M_\infty \times \sin \alpha$ ) on aerodynamic characteristics of simple-shape bodies was studied in various experiments [7-15].

The Reynolds number  $Re_0$  can be considered as the unique main similarity parameter for modeling hypersonic flows in all three flow regimes: continuum, transitional and free-molecular. Using this criterion and other similarity parameters mentioned above, it is possible to perform other well-known parameters [2, 3, 5]. For example, in continuum regime, the parameter  $Re_0$  defines both the

interaction parameter  $P$  for pressure approximation and the viscous-interaction parameter  $V$  for skin-friction approximation [7]. The Reynolds number  $Re_0$  also scales the flow rarefaction, which is characterized by the Knudsen number  $Kn_L$  [6, 14], as well as by the viscous-interaction parameter  $V$  [3, 5, 7].

In the present study, the influence of similarity parameters  $Re_0$ ,  $t_w$ ,  $\gamma$ ,  $n$ ,  $M_\infty$ , and  $K_\infty = M_\infty \times \sin 2$  on the aerodynamic characteristics ( $C_x$ ,  $C_y$ , and  $C_{m0}$ ) has been examined. The characteristics of plates, wedges, disks, and sharp cones have been investigated in rarefied flows of helium, argon, nitrogen, and air under test conditions in a vacuum chamber at Knudsen numbers  $Kn$  from 0.002 to 7. Numerical results have been obtained by the Direct Simulation Monte Carlo [DSMC] technique [14] using DS2G computer code developed by Bird [16]. The calculated results have been compared with experimental data, which were obtained by the author and his colleagues [6-10].

The aerodynamic coefficients of a spinning infinite cylinder [17] have been evaluated numerically for a range of similarity parameters: Knudsen number  $Kn_D$  and spin rate  $W$ . It has been found that the lift force on a spinning cylinder at subsonic upstream conditions has different signs in the free-molecule and continuum regimes. The location of the sign change is in the transitional regime at  $Kn_D = 0.1$ .

The effect of physical and chemical nonequilibrium on simulation of hypersonic rarefied-gas flows over blunt bodies has been studied by solving the full Navier-Stokes equations [18] and the viscous-shock-layer equations [19]. The “frozen”, non-equilibrium, and equilibrium flow regimes have been examined for various physical and chemical processes in air and nitrogen, including excitation of rotational degrees of molecular freedom, as well as dissociation, chemical reactions, and ionization [20-22]. It has been found that the binary similitude law [22, 23] is satisfied for blunt bodies in the transition flow regime of dissociating and ionizing gases under hypersonic vehicle flight conditions at altitudes from 60 to 110 km.

## 2 Aerodynamics of Simple-Shape Bodies

### 2.1 Influence of Mach number

The study of the influence of Mach number  $M_\infty$  on the aerodynamic characteristics of bodies of simple shape has been conducted at small values of the Reynolds number and at constant values of similarity parameters:  $Re_0$ ,  $t_w$ ,  $\gamma$ , and  $n$ . The regime of hypersonic stabilization [5] will occur at  $M_\infty \theta \gg 1$  in the case of streamlining of the thin bodies when the angle  $\theta$  between the generatrix of the body surface and the direction of the upstream flow becomes small enough. This regime will be realized at smaller values of  $M_\infty$ , if the angle  $\theta$  increases.

The dependence of lift-drag ratio for a wedge ( $\theta = 20$  deg) on the angle of attack has been studied in numerical simulations of helium flow at  $Re_{0,L} = 4$ ,  $t_w = 1$  and different values of the freestream Mach number. The DSMC results are shown in Fig. 1 for  $M_\infty = 9.9$  (circles) and  $M_\infty = 11.8$  (squares), correspondingly and indicate a weak dependency of aerodynamic coefficients on  $M_\infty$  in this flow regime. The base area of the wedge and its length were taken as the reference area and length. The numerical results correlate well with the experimental data [8-10] (empty circles and squares), which were obtained in a vacuum wind tunnel at the same flow parameters. In the free-molecular flow regime, the characteristics are not sensitive to changes in upstream flow parameters at  $M_\infty > 9$  [24]. Another interesting fact is that the lift-drag ratio in the transitional flow regime is larger by 50% than the corresponding parameter in the free-molecular regime (see, also, Refs. 6-10).

The results indicate that the hypersonic flow independency principle [5] is realized in the transitional rarefied flow regime [6-10] at  $K = M_\infty \times \sin \theta > 1$ . As was found in experiments [6-10], this principle is not true for thin bodies at small angles of attack in rarefied gas flows under the conditions  $K < 1$ .

The drag coefficient of a blunt plate having relative thickness  $\delta = h/L = 0.06$  becomes sensitive to the magnitude of the freestream Mach number in helium flow (Fig. 2,  $M_\infty = 7.5$

and  $M_\infty = 10.7$ ) at small angles of attack  $\alpha < 12$  deg. The results calculated by the DSMC technique (filled markers) correlate well with the experimental data [8-10] (empty markers). For the lift coefficient, the free-molecular flow data [24], as well as computational and experimental results presented in Fig. 3, are independent of the Mach number, and the value  $C_{y,FM}$  is less by approximately 15% than the value  $C_y$  for transitional flow regime at  $\alpha > 16$  deg. This phenomenon was discussed in Ref. 9.

## 2.2 Influence of the specific heat ratio $\gamma$

In the free-molecular flow regime, the influence of the specific heat ratio  $\gamma$  on the aerodynamic characteristics of bodies depends on the normal component of the momentum of the reflected molecules, which is a function of  $\gamma$  [7, 9]. The same phenomenon can be observed at the transitional conditions in the case of the disk at  $\alpha = 90$  deg. The nitrogen-argon pair was the most acceptable one for testing [8-10]. The dependencies of  $C_x$  of the disc for Ar (filled triangles) and  $N_2$  (filled squares) are shown in Fig. 4 for a wide range of Reynolds number ( $Re_0$ ). At the same parameters of the upstream flow, numerical data obtained by the DSMC technique for different models of molecules are compared with experimental data [8, 9].

The influence of specific heat ratio on the drag coefficient is more significant for small values of  $Re_0 < 10$ . In the free molecular regime ( $Re_0 < 0.2$ ) an increase of  $C_x$  is observed as  $\gamma$  increases [8, 24]. This increase is caused by the dependence on  $\gamma$  of the reflected momentum of the molecules at  $t_w = 1$ . The degree of this influence has been evaluated as 8% at  $Re_0 < 3$ . As the number  $Re_0$  increases, this influence decreases, and at  $Re_0 > 10$ , the drag coefficient of the disk in diatomic gas (nitrogen) becomes larger than that for a monatomic gas. In the continuum flow regime, the dependence of the drag-coefficient on  $\gamma$  difference is insignificant.

The influence of the specific heat ratio  $\gamma$  on the drag coefficient of thin bodies in the transitional flow regime was studied by Gusev et al [8, 9] and Riabov [7, 10] for a sharp wedge ( $\theta = 20$  deg). This effect is estimated as 4% (see

Figs. 5-7). In the hypersonic limit [5] at  $M_\infty \gg 1$ , the drag coefficient of thin bodies will be proportional to  $(\gamma + 1)$ . The accuracy of experimental data in the range  $1 < Re_0 < 70$  has been estimated as 10%.

## 2.3 Influence of the viscosity parameter $n$

The helium-argon pair is considered for evaluating the influence of the viscosity parameter  $n$ , which is used in the approximation of the viscosity coefficient  $\mu \sim T^n$ . It is noted that the exponent  $n$  is closely related to the exponent  $s$  in the exponential law of molecular interaction [8]. The exponents  $n$  for argon and helium have approximately constant values and differ significantly ( $n_{Ar} = 0.87$  and  $n_{He} = 0.64$ ) at  $T < 300$  K. The calculating of flow parameters near the disk at  $\alpha = 90$  deg (see Fig. 4) was conducted in these gases (triangles for Ar and circles for He). The experimental data [8, 9] (empty markers) indicates that an insignificant increase (5%) of  $C_x$  occurs with the increase of  $n$  at  $Re_0 < 10$ . At the same time, the accuracy of experimental data in the range  $1 < Re_0 < 60$  has been estimated as 8%. In free-molecular and continuum flow regimes, this phenomenon is negligible (see the dashed lines in Fig. 4).

## 2.4 Influence of the Temperature Factor $t_w$

Compared to other similarity parameters, the temperature factor ( $t_w = T_w/T_0$ ) is the most important [4, 6-9]. As an example, numerical data for aerodynamic coefficients of a plate ( $\delta = 0.06$ ) are shown in Figs. 5-7 for wide range of Reynolds numbers. The lift coefficient changes non-monotonically from the continuum to the free-molecular flow regime (see Fig. 6). Maximum values occur in the transitional flow regime. The influence of the temperature factor can be estimated as 8% for the drag coefficient and as 25% for the lift coefficient. The results correlate well with the experimental data [8, 9]. Decreasing the temperature factor significantly decreases the pressure at the body surface in comparison with the tangential stresses [7, 9]. Therefore, the lift and pitch moment coefficients are the most sensitive aerodynamic parameters

to changes of  $t_w$  in the transitional and free-molecular flow regimes (see Fig. 6).

The temperature factor effect on the drag coefficient of a thin body has been studied numerically for a sharp cone with semiangle  $\theta_c = 10$  deg at  $\alpha = 0$  deg in air (Fig. 8). It was found, that at  $t_w = 0.43$  and  $Re_\theta < 30$ , the drag coefficient is 5-10% lower compared to that for a "hot" wall ( $t_w = 1$ ). The numerical data are compared with the experimental data of Gusev et al [9]. Both sets of data correlate well at  $Re_\theta < 0.8$  and  $Re_\theta > 10$ . The maximum value of the drag coefficient at  $Re_\theta \sim 3$  and  $t_w = 0.43$  has not been found in calculations. One of the reasons of this difference is the non-uniform flow condition in experiments with underexpanded jets (see Refs. 8-10). At small values of the cone semiangle  $\theta_c = 10$ deg and non-uniform-flow conditions, the usage of the average Reynolds number  $Re_\theta$  can generate additional errors related to approximation procedures.

### 3 Aerodynamics of a Spinning Cylinder

#### 3.1 Subsonic rarefied-gas-flow regime

At subsonic flow conditions, the speed ratio  $S = M_\infty \cdot (0.5 \cdot \gamma)^{1/2}$  becomes small, and aerodynamic coefficients become very sensitive to its magnitude [17, 25]. In the present paper, the transition flow regime has been studied numerically at  $M_\infty = 0.15$ ,  $\gamma = 5/3$  (argon gas), and spin ratio  $W = 1, 3$  and  $6$ .

The lift and drag coefficients are shown in Figs. 9 and 10, respectively. In the transition flow regime ( $Kn_D > 0.03$ ), both the incident and reflected molecules significantly influence the lift [17]. The incident molecules dominate when  $Kn_D < 0.1$ , and the reflected molecules dominate when  $Kn_D > 0.1$ . Under these conditions, the lift coefficient changes sign for the cylinder spinning in counter-clockwise direction, and the drag coefficient becomes a function of the spin rate [25]. The flow-field patterns near a spinning cylinder at near-free-molecule ( $Kn_D = 3.18$ ) and near-continuum ( $Kn_D = 0.032$ ) flow regimes were studied in Ref. 17. The character of the flow is absolutely different in these cases.

The zone of circulating flow is much wider in continuum-flow regime, and its width is comparable with the radius of a cylinder. In the near-free-molecule flow regime, the asymmetry of the flow in upper and bottom regions is significant. The major disturbances of the flow parameters are concentrated in the vicinity of the spinning surface. In the opposite case of near-continuum flow regime, the spinning effect changes significantly the flow pattern in the area far from the surface. These differences in flow patterns dominate the character of molecule-surface interactions.

#### 3.2 Subsonic rarefied-gas-flow regime

At supersonic flow conditions, the speed ratio  $S$  becomes large, and the aerodynamic coefficients become less sensitive to its magnitude [17, 25]. In the present study, the transition flow regime has been investigated numerically at  $M_\infty = 10$ ,  $\gamma = 5/3$  (argon gas), and spin ratio  $W = 0.03$  and  $W = 0.1$ .

The lift and drag coefficients are shown in Figs. 11 and 12, respectively. For the lift coefficient, the influence of reflected molecules is dominant in the transition-flow regime ( $Kn_D > 0.03$ ). The incident-molecule input becomes significant at Knudsen number  $Kn_D < 0.1$  [17]. Under the considered flow conditions, the lift coefficient has a positive sign (which is opposite to the sign under the continuum flow regime) for the cylinder spinning in a counter-clockwise direction. The drag coefficient is insensitive to the spin rate. The values of  $C_x$  and  $C_x$  at  $Kn_D > 4$  are near the magnitudes of the coefficients for the free-molecule flow [25].

The flow characteristics are different in these cases [17]. For a small spin rate,  $W=0.1$ , the zone of circulating flow is located in the vicinity of the surface, and it does not affect the flow zone located far from the surface. The flow pattern becomes asymmetrical. These differences in flow patterns dominate the character of molecule-surface interactions, and they characterize the differences in the performance parameters under significantly distinct flow conditions (see Figs. 11 and 12).

## 4 Solutions of the Navier-Stokes Equations

Another approach that is based on the numerical solutions of the Navier-Stokes equations [18] is widely used in the high-altitude aerodynamics. In present study, the range of applicability and accuracy of the numerical solutions have been analyzed for perfect-gas and nonequilibrium flows near blunt bodies [18-20]. Numerical solutions are compared with experimental data.

### 4.1 Pressure at the stagnation point

It was noticed by many researchers (see bibliography in Ref. 26) using pressure probes for measuring parameters of supersonic rarefied gas flows, that a significant increase in the measured pressure  $p_w$  over the value  $p_o$  becomes evident when the value of the Reynolds number  $Re_o$  gets smaller. It was found [26], that this phenomenon occurs both on cooled and on thermally isolated probe surfaces, and, in the last case, the quantity of the difference is higher. It was also noted that a monatomic gas has a tendency for a lower level than a diatomic gas. Numerical results for gases with various probe surface temperatures and specific heat ratios  $\gamma$  are shown in Fig. 13. The calculations were made using parameters changing in the range of  $6 < Re_o < 180$ ,  $3.8 < M_\infty < 12$ , and  $0.19 < t_w < 1$ . The comparison of the experimental [26] and computational data favorably indicates a satisfactory correlation between each other.

### 4.2 Rotational-translational relaxation in viscous flows of nitrogen near a sphere

In the present study, the rotational-relaxation effects have been studied in the flow of nitrogen near a front area of a sphere. The full system of the Navier-Stokes equations and the relaxation equation, based on  $\tau$ -approximation technique [20], has been solved by the implicit numerical technique described in Ref. [18]. A significant difference between rotational and translational temperature distributions was found.

The distribution of the nonequilibrium rotational ( $T_R$ , squares) and translational ( $T_t$ , triangles) temperatures are shown in Figs. 14-15 for two cases of rarefied upstream flow: a)

Knudsen number  $Kn_{\infty,R} = 0.08$  (or Reynolds number  $Re_{o,R} = 16.86$ ), Mach number  $M_\infty = 9$ , stagnation temperature  $T_0 = 298$  K, and temperature factor  $t_w = 0.3$ , and b)  $Kn_{\infty,R} = 0.017$  ( $Re_{o,R} = 57.4$ ),  $M_\infty = 18.8$ ,  $T_0 = 1600$  K,  $t_w = 0.19$ . In the viscous shock layer near a sphere, a significant difference between the translational and rotational temperatures can be observed. The shock-layer thickness becomes bigger under the nonequilibrium flow conditions than in the case of “equilibrium” flow at  $T_R = T_t$  (see circles in Figs. 14-15). The numerical results for  $T_R$  correlate well with the experimental data of Tirumalesa [27] and Ahouse and Bogdonoff [28], obtained in wind tunnels by the electron-beam diagnostics.

## 5 Thin-Viscous-Shock-Layer Approximation

The model of a thin viscous shock layer [TVSL] is broadly used for the description of the structure of non-equilibrium viscous gas flow near blunt bodies or hypersonic vehicles [2, 19, 21, 22]. In the present study, the values of the Stanton numbers  $St$  at the stagnation point were calculated at various Reynolds numbers  $Re_o$  and temperature factor  $t_w = 0.033$ . The comparison between the results from the TVSL (triangles) model and the solutions of the complete system of the Navier-Stokes equations with slip (solid squares) and non-slip (empty squares) boundary conditions is shown in Fig. 16. The results correlate well with the experimental data [29].

### 5.1 Nonequilibrium chemically reacting flows

The non-equilibrium, equilibrium and “frozen” flow regimes have been examined for various physical and chemical processes in air, including dissociation, chemical reactions, and ionization [19-22]. It has been found [22], that the catalytic surface reactions have no effect on the pressure and friction distributions over the body. The largest effect on heat transfer and distribution of species concentrations is that of non-equilibrium dissociation and ionization near the non-catalytic surfaces. This effect can be estimated from the curves of the Stanton number at the stagnation point of the body as a

function of Reynolds number (crosses), shown in Fig. 16. The calculations were made for  $u_\infty = 7.8$  km/s and  $R = 1$  m.

## 5.2 Binary simulation law

The numerical results [19, 21, 22] show that the gasdynamic parameters in the TVSL are “frozen” at small values of the Reynolds number,  $Re_o < 20$ . In these cases, the recombination processes are insignificant and the approximate simulation principle of the “binary similitude law” [23],  $\rho_\infty R = const$ , can be applied at  $u_\infty = const$ . Calculations performed for the critical streamline assuming  $u_\infty = 7.8$  km/s,  $\rho_\infty R = 5.35 \cdot 10^{-7}$  kg/m<sup>2</sup> ( $Re_o = 7.33$ ) and nose radii  $R = 1$  m and  $R = 0.005$  m have shown that distributions of flow variables and species concentrations for these two cases are correlated satisfactorily. The results of these calculations for temperature and electron concentration  $N_e$  near catalytic and non-catalytic surfaces are shown in Figs. 17-19.

## Conclusions

New information about hypersonic viscous rarefied gas flows near simple-shape bodies has been obtained and can be effectively used for prediction of aerothermodynamic characteristics of hypersonic vehicles during the design of their missions in complex rarefied atmospheric conditions of the Earth and other planets. For conditions approaching the hypersonic limit, the Reynolds number ( $Re_\theta$ ) and temperature factor ( $t_w$ ) are the primary similarity parameters. The influence of other parameters (the specific heat ratio, viscosity parameter and Mach number) is significant at  $M_\infty \times \sin \alpha < 1$  and  $Re_\theta < 10$ .

The aerodynamic coefficients of a spinning infinite cylinder have been evaluated numerically for a range of two similarity parameters: Knudsen number and spin rate. It has been found that the lift force on a spinning cylinder at subsonic upstream conditions has different signs in the continuum and free-molecule flow regimes. The location of the sign change is in the transitional flow regime near  $Kn_D = 0.1$ . The major factor of influence is the

magnitude of momentum of the reflected and incident molecules, which depends on the value of the Knudsen number. At the upstream supersonic flow conditions, the lift coefficient has a positive sign in the transitional and free molecular regimes (which is opposite to the sign under the continuum flow regime) for the cylinder spinning in a counter-clockwise direction. The supersonic drag coefficient is insensitive to the spin rate, and the incident component dominates the magnitude of  $C_x$ .

The results of this study confirm the hypothesis about the applicability of the Navier-Stokes equations and approximation of a thin viscous shock layer for the description of non-equilibrium rarefied gas flows near the blunt bodies. The binary similitude law can be applied in the studies of the non-equilibrium flows at small values of the Reynolds number,  $Re_o < 20$ .

## Acknowledgments

The author would like to express gratitude to G. A. Bird for the opportunity of using the DS2G computer program, and to V. N. Gusev, A. I. Erofeev, T. V. Klimova, V. K. Molodtsov, V. A. Perepukhov, and V. P. Provotorov for their fruitful participation in developing methods for solution of the problem.

## References

- [1] Gnoffo P. Planetary-entry gas dynamics. *Annual Review of Fluid Mechanics*, Vol. 31, pp. 459-494, 1999.
- [2] Cheng H. Perspectives on hypersonic viscous flow research. *Annual Review of Fluid Mechanics*, Vol. 25, pp. 455-484, 1993.
- [3] Koppenwallner G. Fundamentals of hypersonics: aerodynamics and heat transfer. *Hypersonic Aerothermodynamics*, Deutsche Forschungs- und Versuchsanstalt für Luft- und Raumfahrt E. V., Lecture Series, No. 1984-01, DFVLR-Press, 1984.
- [4] Gusev V. High-altitude aerothermodynamics, *Fluid Dynamics*, Vol. 28, No. 2, pp. 269-276, 1993.
- [5] Anderson J. *Hypersonic and high temperature gas dynamics*. 1st edition, McGraw-Hill, 1989.
- [6] Gusev V, Kogan M and Perepukhov V. The similarity and aerodynamic measurements in transitional regime at hypersonic speeds. *Uchenyye Zapiski TsAGI*, Vol. 1, No. 1, pp. 24-31, 1970 (in Russian).

- [7] Riabov V. Comparative similarity analysis of hypersonic rarefied gas flows near simple-shape bodies. *Journal of Spacecraft and Rockets*, Vol. 35, No. 4, pp. 424-433, 1998.
- [8] Gusev V, Klimova T and Riabov V. The main regularities of aerodynamic characteristics changes in the transitional regimes of hypersonic flows. *Uchenyye Zapiski TsAGI*, Vol. 7, No. 3, pp. 47-57, 1976 (in Russian).
- [9] Gusev V, Erofeev A, Klimova T, Perekukhov V, Riabov V and Tolstykh A. Theoretical and experimental investigations of flow over simple shape bodies by a hypersonic stream of rarefied gas. *Trudy TsAGI*, No. 1855, pp. 3-43, 1977 (in Russian).
- [10] Riabov V. Aerodynamic applications of underexpanded hypersonic viscous jets. *Journal of Aircraft*, Vol. 32, No. 3, pp. 471-479, 1995.
- [11] Legge H. Force and heat transfer measurements in hypersonic free-jet flow. *AIAA Paper*, No. 94-2633, pp. 1-9 1994.
- [12] Dahlen G and Brundin C. Wall temperature effects on rarefied hypersonic cone drag. *Proc. 13th International Symposium on Rarefied Gas Dynamics*, Novosibirsk, Vol. 1, pp. 453-460, 1985.
- [13] Lengrand J, Allège J, Chpoun A and Raffin M. Rarefied hypersonic flow over a sharp flat plate: numerical and experimental results. *Rarefied Gas Dynamics: Space Science and Engineering*, Vol. 160, *Progress in Astronautics and Aeronautics*, AIAA, Washington, DC, pp. 276-284, 1994.
- [14] Bird G. *Molecular gas dynamics and the direct simulation of gas flows*. 1st edition, Oxford University Press, 1994.
- [15] Gusev V, Erofeev A, Provotorov V and Yegorov I. Numerical simulation and experiment in rarefied gas dynamics. *Proc. 20th International Symposium on Rarefied Gas Dynamics*, Inst. of Mechanics, Chinese Academy of Sciences, Beijing, PRC, p. E1, 1996.
- [16] Bird G. *The DS2G program user's guide, version 3.2*. G. A. B. Consulting Pty Ltd., Killara, New South Wales, Australia, pp. 1-56, 1999.
- [17] Riabov V. Aerodynamics of a spinning cylinder in rarefied gas flows. *Journal of Spacecraft and Rockets*, Vol. 36, No. 3, pp. 486-488, 1999.
- [18] Molodtsov V and Riabov V. Investigation of the structural features of rarefied gas flows about a sphere using Navier-Stokes equations. *Proc. 13th International Symposium on Rarefied Gas Dynamics*, Novosibirsk, Vol. 1, pp. 535-541, 1985.
- [19] Riabov V and Provotorov V. The structure of multicomponent nonequilibrium viscous shock layers. *AIAA Paper*, No. 94-2054, pp. 1-8, 1994.
- [20] Riabov V. Gas dynamic equations, transport coefficients, and effects in nonequilibrium diatomic gas flows. *Journal of Thermophysics and Heat Transfer*, Vol. 14, No. 3, pp. 404-411, 2000.
- [21] Provotorov V and Riabov V. Effect of chemical reactions on the flow of air in a viscous shock layer. *Fluid Mechanics - Soviet Research*, Vol. 12, No. 6, pp. 17-25, 1983.
- [22] Gusev V, Provotorov V and Riabov V. Effect of physical and chemical nonequilibrium on simulation of hypersonic rarefied-gas flows. *Fluid Mechanics - Soviet Research*, Vol. 10, No. 5, pp. 123-135, 1981.
- [23] Agafonov V *et al.* *Nonequilibrium physico-chemical processes in aerodynamics*. Mashinostroeniye, 1972 (in Russian).
- [24] Kogan M. *Rarefied gas dynamics*. Plenum Press, 1969.
- [25] Ivanov S and Yanshin A. Forces and moments acting on bodies rotating about a symmetry axis in a free molecular flow. *Fluid Dynamics*, Vol. 15, No. 3, pp. 449-453, 1980.
- [26] Chue S. Pressure probes for fluid measurement. *Progress in Aerospace Science*, Vol. 16, No. 2, pp. 147-223, 1975.
- [27] Tirumalesa D. An experimental study of hypersonic rarefied flow over a blunt body. *AIAA Journal*, Vol. 6, No. 2, pp. 369-370, 1968.
- [28] Ahouse D and Bogdonoff S. An experimental flow field study of the rarefied blunt body problem. *AIAA Paper* 69-656, 1969.
- [29] Ardasheva M, Klimova T, Pervushin G and Chernikova L. Application of a two-layer thermal-indicator coating for investigating heat transfer in vacuum wind tunnels. *Uchenyye Zapiski TsAGI*, Vol. 10, No. 6, 1979, pp. 79-87 (in Russian).

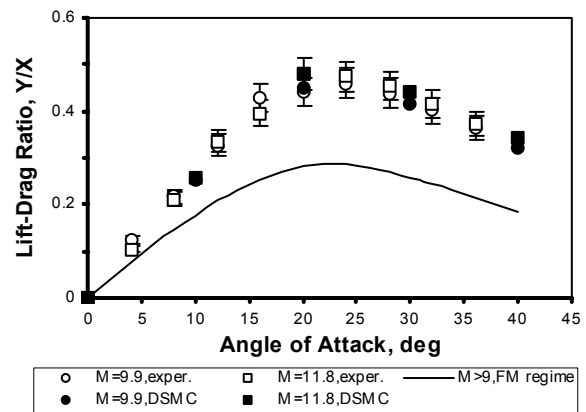


**Fig. 1** Lift-drag ratio  $Y/X$  for a wedge ( $\theta = 20$  deg) in helium flow at  $Re_\theta = 4$  and  $M_\infty = 9.9$  and 11.8. Experimental data from Refs. 8-10.

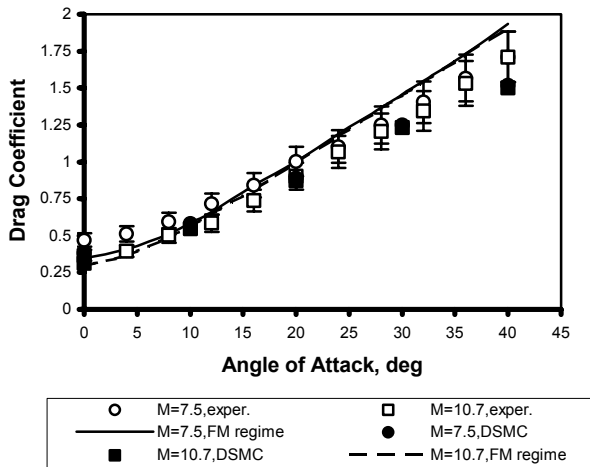


Fig. 2 Drag coefficient  $C_x$  for a blunt plate ( $\delta = 0.06$ ) at  $Re_0 = 2.46$  and  $M_\infty = 7.5$  (circles) and 10.7 (squares) in helium. Experimental data from Refs. 8-10.

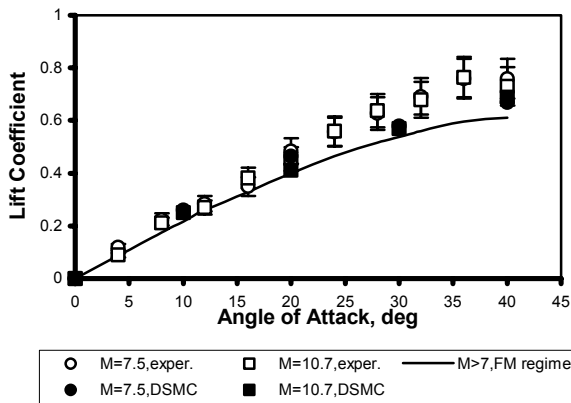


Fig. 3 Lift coefficient  $C_y$  for a blunt plate ( $\delta = 0.06$ ) at  $Re_0 = 2.46$  and  $M_\infty = 7.5$  (circles) and 10.7 (squares) in helium. Experimental data from Refs. 8-10.

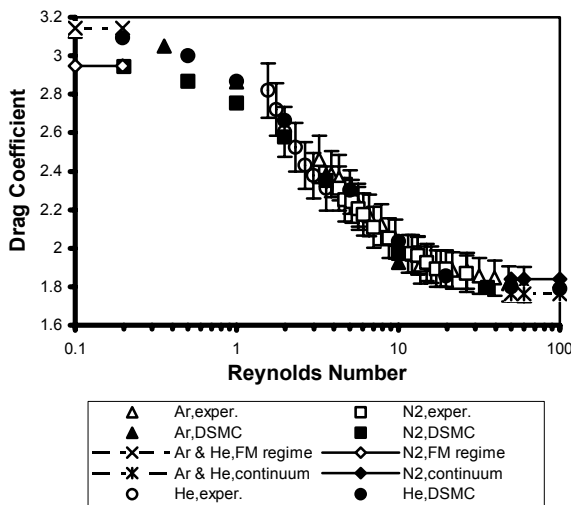


Fig. 4 Drag coefficient  $C_x$  for a disk ( $\alpha = 90$  deg) vs Reynolds number  $Re_0$  in argon (triangles), helium (circles), and nitrogen (squares). Experimental data from Refs. 8 and 9.

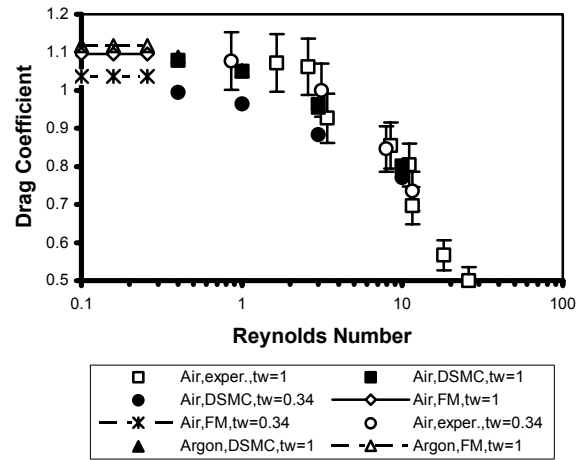


Fig. 5 Drag coefficient  $C_x$  for a blunt plate ( $\delta = 0.1$ ) vs Reynolds number  $Re_0$  in air and argon at  $\alpha = 20$  deg. Experimental data from Ref. 9.

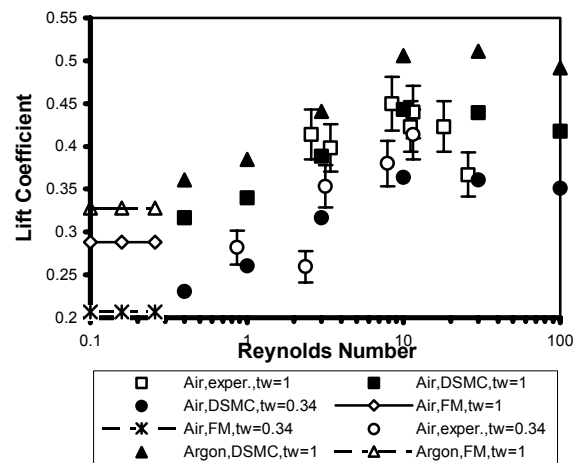


Fig. 6 Lift coefficient  $C_y$  for a blunt plate ( $\delta = 0.1$ ) vs Reynolds number  $Re_0$  in air and argon at  $\alpha = 20$  deg. Experimental data from Ref. 9.

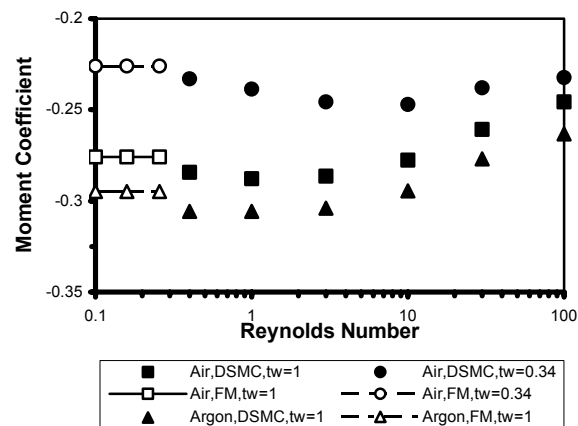


Fig. 7 Pitch moment coefficient  $C_{m0}$  for a blunt plate ( $\delta = 0.1$ ) vs Reynolds number  $Re_0$  in air and argon at  $\alpha = 20$  deg. Experimental data from Ref. 9.

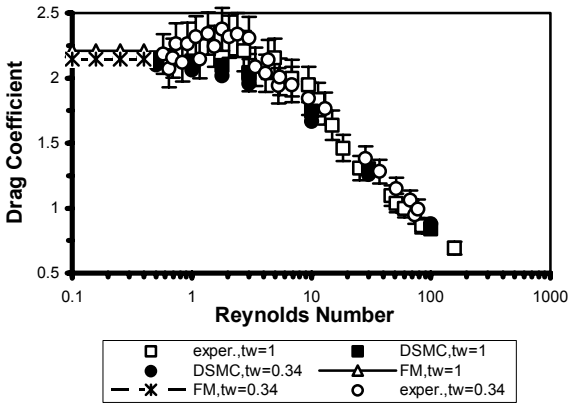


Fig. 8 Drag coefficient  $C_x$  for a sharp cone ( $\theta_c = 10$  deg) in air at  $\alpha = 0$  deg and different temperature factors:  $t_w = 1$  and  $t_w = 0.34$ . Experimental data from Ref. 9.

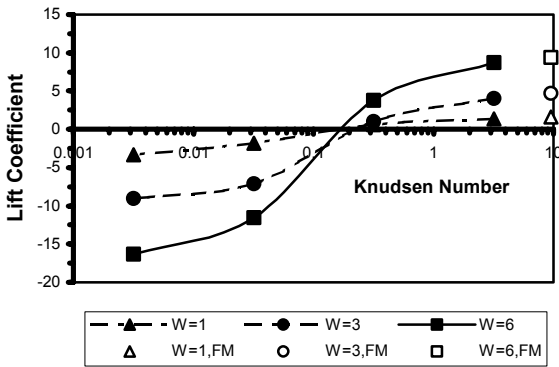


Fig. 9 Lift coefficient  $C_y$  of a spinning cylinder vs Knudsen number  $Kn_D$  at  $M_\infty = 0.15$  and different spin rates  $W$  in argon.

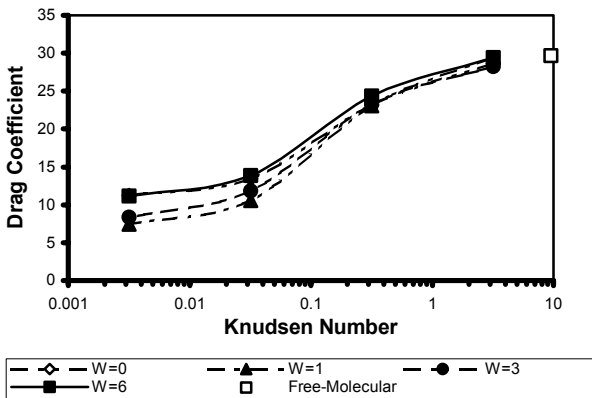


Fig. 10 Drag coefficient  $C_x$  of a spinning cylinder vs Knudsen number  $Kn_D$  at  $M_\infty = 0.15$  and different spin rates  $W$  in argon.

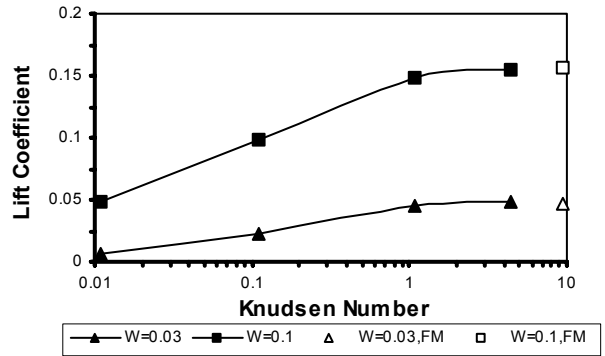


Fig. 11 Lift coefficient  $C_y$  of a spinning cylinder vs Knudsen number  $Kn_D$  at  $M_\infty = 10$  and different spin rates  $W$  in argon.

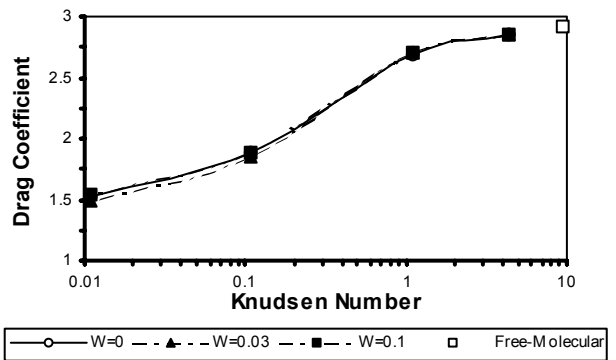


Fig. 12 Drag coefficient  $C_x$  of a spinning cylinder vs Knudsen number  $Kn_D$  at  $M_\infty = 10$  and different spin rates  $W$  in argon.

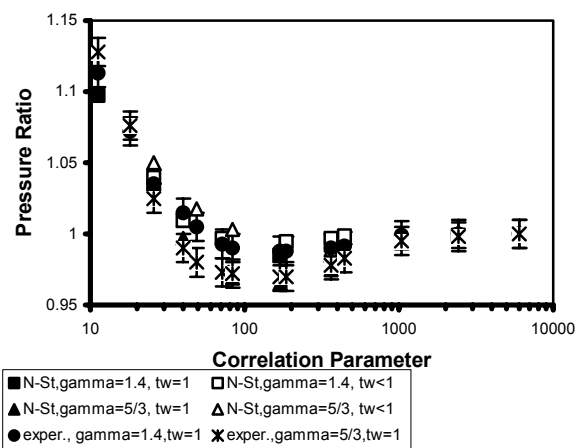


Fig. 13 Pressure ratio  $p_w/p_o$  at the front stagnation point of a sphere vs correlation parameter  $Re_s(\rho_s/\rho_\infty)^{1/2}$ .

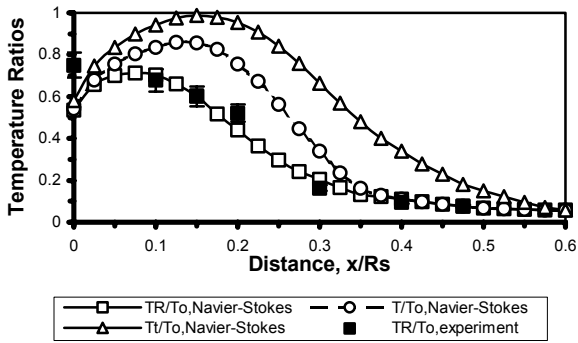


Fig. 14 The nonequilibrium rotational  $T_R$ , translational  $T_t$ , and equilibrium overall  $T$  temperatures at the stagnation stream line near a sphere:  $Kn_{\infty,R} = 0.08$  ( $Re_{\theta,R} = 16.86$ ),  $M_{\infty} = 9$ ,  $T_0 = 298$  K,  $t_w = 0.3$ . Experimental data from Ref. 27.

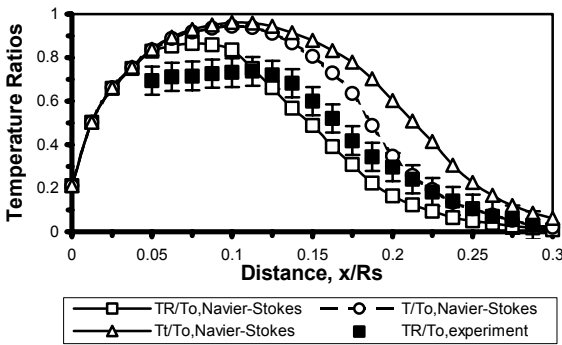


Fig. 15 The nonequilibrium rotational  $T_R$ , translational  $T_t$ , and equilibrium overall  $T$  temperatures at the stagnation stream line near a sphere:  $Kn_{\infty,R} = 0.017$  ( $Re_{\theta,R} = 57.4$ ),  $M_{\infty} = 18.8$ ,  $T_0 = 1600$  K,  $t_w = 0.19$ . Experimental data from Ref. 28.

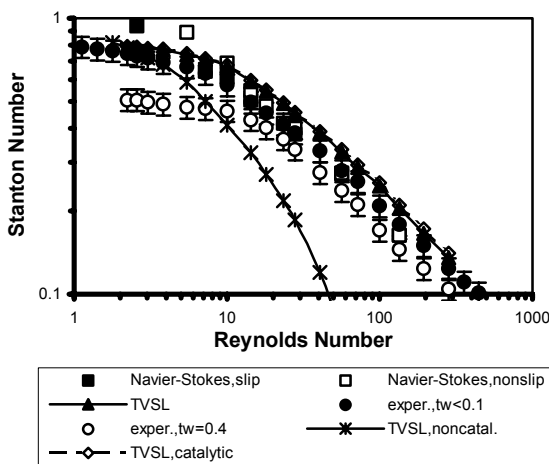


Fig. 16 Stanton numbers  $St$  vs Reynolds numbers  $Re_{\theta,R}$  for different medium models. Experimental data from Ref. 29.

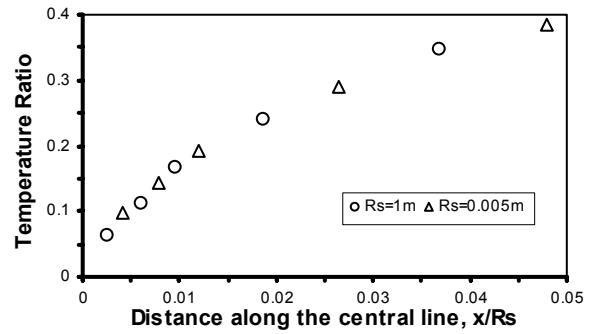


Fig. 17 Temperature  $T/T_0$  at the stagnation streamline of the sphere at  $Re_{\theta,R} = 7.33$ ,  $u_{\infty} = 7.8$  km/s,  $\rho_{\infty}R_s = 5.35 \cdot 10^{-7}$  kg/m<sup>2</sup> and different sphere radii:  $R_s = 1$  and  $R_s = 0.005$ m.

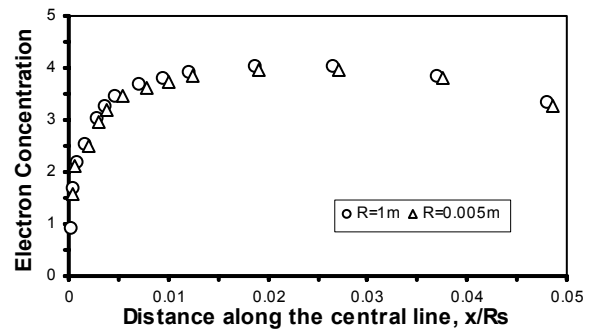


Fig. 18 Electron concentration  $N_e \cdot R_s \cdot 10^{-11}$  m<sup>-2</sup> at the stagnation streamline of the sphere at  $Re_{\theta,R} = 7.33$ ,  $u_{\infty} = 7.8$  km/s,  $\rho_{\infty}R_s = 5.35 \cdot 10^{-7}$  kg/m<sup>2</sup> and different sphere radii:  $R_s = 1$  and  $R_s = 0.005$ m. Catalytic surface.

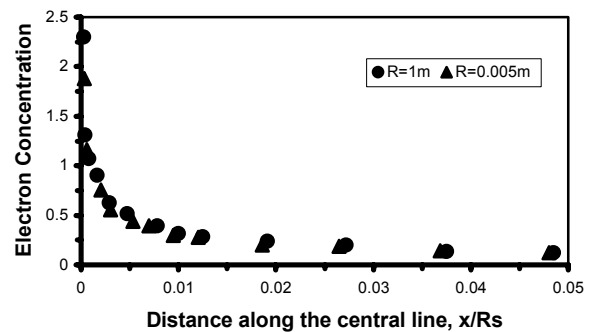


Fig. 19 Electron concentration  $N_e \cdot R_s \cdot 10^{-14}$  m<sup>-2</sup> at the stagnation streamline of the sphere at  $Re_{\theta,R} = 7.33$ ,  $u_{\infty} = 7.8$  km/s,  $\rho_{\infty}R_s = 5.35 \cdot 10^{-7}$  kg/m<sup>2</sup> and different sphere radii:  $R_s = 1$  and  $R_s = 0.005$ m. Noncatalytic surface.